Role of pre-existing structures in controlling the Cenozoic tectonic evolution of the eastern Tibetan plateau: New insights from analogue experiments

Ming Sun [a], An Yin [a,b,*], Danping Yan [a,**], Hongyu Ren [a], Hongxu Mu [a], Lutao Zhu [a,c], Liang Qiu [a]

[a] *School of Earth Sciences and Resources, China University of Geosciences, Beijing 100083, China*
[b] *Department of Earth, Planetary, and Space Sciences, University of California, Los Angeles, CA 90095-1567, USA*
[c] *7th Gold Exploration Team of the Chinese Armed Police Force, Yantai 264004, China*

A B S T R A C T

Pre-existing weakness due to repeated tectonic, metamorphic, and magmatic events is a fundamental feature of the continental lithosphere on Earth. Because of this, continental deformation results from a combined effect of boundary conditions imposed by plate tectonic processes and heterogeneous and anisotropic mechanical strength inherited from protracted continental evolution. In this study, we assess how this interaction may have controlled the Cenozoic evolution of the eastern Tibetan plateau during the India–Asia collision. Specifically, we use analogue models to evaluate how the pre-Cenozoic structures may have controlled the location, orientation, and kinematics of the northwest-striking Xianshuihe and northeast-striking Longmen Shan fault zones, the two most dominant Cenozoic structures in eastern Tibet. Our best model indicates that the correct location, trend, and kinematics of the two fault systems can only be generated and maintained if the following conditions are met: (1) the northern part of the Songpan–Ganzi terrane in eastern Tibet has a strong basement whereas its southern part has a weak basement, (2) the northern strong basement consists of two pieces bounded by a crustal-scale weak zone that is expressed by the Triassic development of a northwest-trending antiform exposing middle and lower crustal rocks, and (3) the region was under persistent northeast–southwest compression since ∼35 Ma. Our model makes correct prediction on the sequence of deformation in eastern Tibet; the Longmen Shan right-slip transpressional zone was initiated first as an instantaneous response to the northeast–southwest compression, which is followed by the formation of the Xianshuihe fault about a half way after the exertion of northeast–southwest shortening in the model. The success of our model highlights the importance of pre-existing weakness, a key factor that has been largely neglected in the current geodynamic models of continental deformation.

1. Introduction

Formation of continental lithosphere results from multi-phase magmatic differentiation, terrane accretion/collision, metamorphism, and tectonic activities (e.g., Hawkesworth et al., 2017). As a result of its protracted evolution, the rheological properties of continental lithosphere vary strongly in time and space, contrasting sharply to those of oceanic lithosphere (e.g., McKenzie et al., 2005). The spatiotemporally variable mechanical strength of the continental lithosphere can be expressed either as crustal-scale weak zones or storage of gravitational potential energy (e.g., Kluth and Coney, 1981; England and Houseman, 1989). Hence, continental deformation is ultimately a combined result of (1) boundary conditions imposed by plate tectonic processes and (2) the interaction of its induced stress fields with pre-existing distribution of heterogeneity and anisotropy inherited from protracted early continental evolution.

The eastern margin of the Tibetan plateau was created by the Cenozoic development of the Longmen Shan thrust belt/right-slip transpressional system during the India–Asia collision. The Longmen Shan thrust belt is located at the site where intense Triassic deformation took place during the closure of the Paleo-Tethys (e.g., Burchfiel and Chen, 2012). Despite this well-established geologic
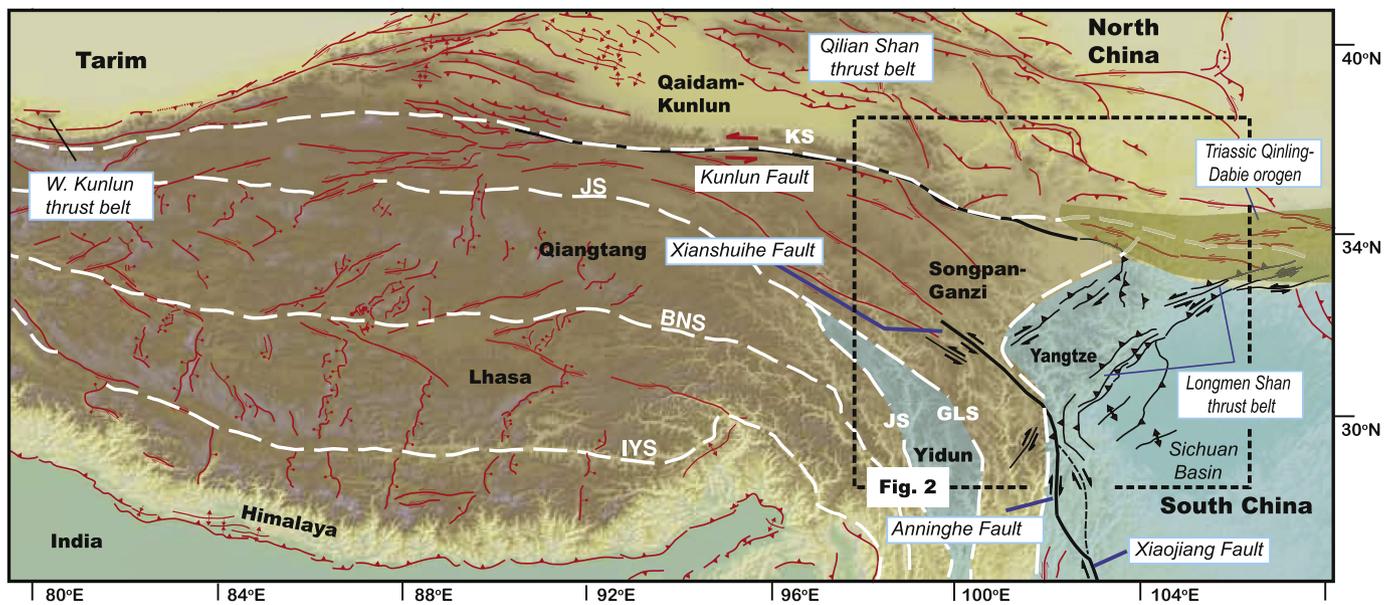
Fig. 1. Cenozoic fault map of the Himalayan–Tibetan orogen and location of major pre-Cenozoic terrane boundaries after Taylor and Yin (2009). IYS: Indus–Yarlung suture; BNS: Bangong–Nujiang suture; JS: Jinsha suture; GLS: Garze–Litang suture; KS: Kunlun suture. Note that the boundary between the Yangtze terrane of South China and the Songpan–Ganzi terrane is transitional and complex due to Triassic and Cenozoic deformation. Also shown is the approximate location of Fig. 2B.

relationship, the dynamic role of Triassic structures in controlling Cenozoic tectonic evolution of the eastern Tibetan plateau has not been investigated. Current research on the Cenozoic development of the eastern Tibetan plateau focuses mainly on testing two end-member models in cross-section view, with one emphasizing the role of lower-crustal channel flow (e.g., Clark and Royden, 2000; Bendick and Flesch, 2007) and another the development of a thrust wedge (e.g., Hubbard and Shaw, 2009). Not only that the above two end-member models do not involve pre-existing weakness, their two-dimensionality makes them inadequate to evaluate the impact of the well-established Cenozoic transpressional and strike-slip faulting on the tectonic development of the eastern Tibetan plateau (Fig. 1).

Although the role of pre-existing weakness in controlling intra-plate deformation at a continental scale has been evaluated through numerical modeling (e.g., Neil and Houseman, 1997; Kong et al., 1997) and the application of rock-mechanics principles (e.g., Cooke and Underwood, 2001; Tong and Yin, 2011), these approaches are unable to simulate coeval nucleation of new faults and reactivation of pre-existing weak zones in the continental lithosphere. This problem can be overcome by analogue modeling that is capable of simulating fault creation and reactivation under proper model setups (e.g., Haq and Davis, 1997; Viola et al., 2004; Yan et al., 2016). In this study we use analogue-model experiments to determine the mechanical origins of the left-slip Xianshuihe fault zone and the right-slip transpressional Longmen Shan belt, the two most dominant Cenozoic fault systems in eastern Tibet. Specifically, we would like to answer the following questions. (1) Was the Xianshuihe fault nucleated as a new structure or reactivated from an older weakness zone? (2) Does the Songpan–Ganzi terrane have a coherent or fragmented basement in eastern Tibet? (3) What has been the dominant shortening direction in eastern Tibet during the development of the Cenozoic Xianshuihe and Longmen Shan fault zones?

2. Geologic setting of eastern Tibet

2.1. Triassic structures

Eastern Tibet exposes the Songpan–Ganzi terrane, the Yidun terrane, and the western margin of the Yangtze terrane/craton

(Fig. 1) (Yin and Nie, 1996; Yin and Harrison, 2000; Roger et al., 2010). The Songpan–Ganzi terrane is composed of a thick (locally >15 km) Triassic turbidite sequence that is strongly folded and intruded by earliest Jurassic plutons (Nie et al., 1994; Burchfiel and Chen, 2012; de Sigoyer et al., 2014). The easternmost Songpan–Ganzi terrane and the Yangtze craton share the same continental basement, which is characterized by the presence of 825–750 Ma felsic rocks (Zhou et al., 2002) covered by Neoproterozoic to Triassic strata (Fig. 2) (Roger et al., 2010). The Yidun terrane is bounded by the Garze–Litang and Jinsha suture zones between the Qiangtang and Songpan–Ganzi terranes (Fig. 1) and consists of a Cambrian–Carboniferous continental-shelf sequence overlain by a Permo-Triassic arc sequence (e.g., Reid et al., 2005; Roger et al., 2010). Geochemistry and Hf model ages of Triassic and Cretaceous plutonic rocks require the Yidun terrane to have a thinned continental basement, which may have resulted from rifting from the Yangtze terrane during the postulated Permian backarc extension (Reid et al., 2005) (Fig. 2A). Deformation of the Yidun terrane was induced by the Early Triassic closure of the Jinsha Ocean in the west side and the Late Triassic closure of the Garze–Litang Ocean on the east side, respectively (Reid et al., 2005; Burchfiel and Chen, 2012) (Fig. 2B).

2.2. Cenozoic structures

The first-order Cenozoic structures in eastern Tibet are the Longmen Shan thrust belt and the Xianshuihe left-slip fault. The northeast-striking Longmen Shan thrust belt defines the eastern margin of the Tibetan plateau (Fig. 1) (Burchfiel et al., 1995), which has experienced slow exhumation during the early Cenozoic followed by two pulses of rapid exhumation at 30–25 and 10–15 Ma, respectively (Wang et al., 2014). The northern segment of the thrust belt accommodates both thrusting and right-slip shear deformation (Fig. 1), whereas the southern segment terminates at the left-slip Xianshuihe fault (Burchfiel et al., 1995; Liu-Zeng et al., 2010; Yan et al., 2011; Burchfiel and Chen, 2012). The Xianshuihe fault has accommodated ∼60 km left-slip offset and has been active since ∼10 Ma (Roger et al., 1995; Burchfiel et al., 1995). This age is significantly younger than the initiation age of the Longmen Shan thrust belt to the north at ∼35 Ma (Wang
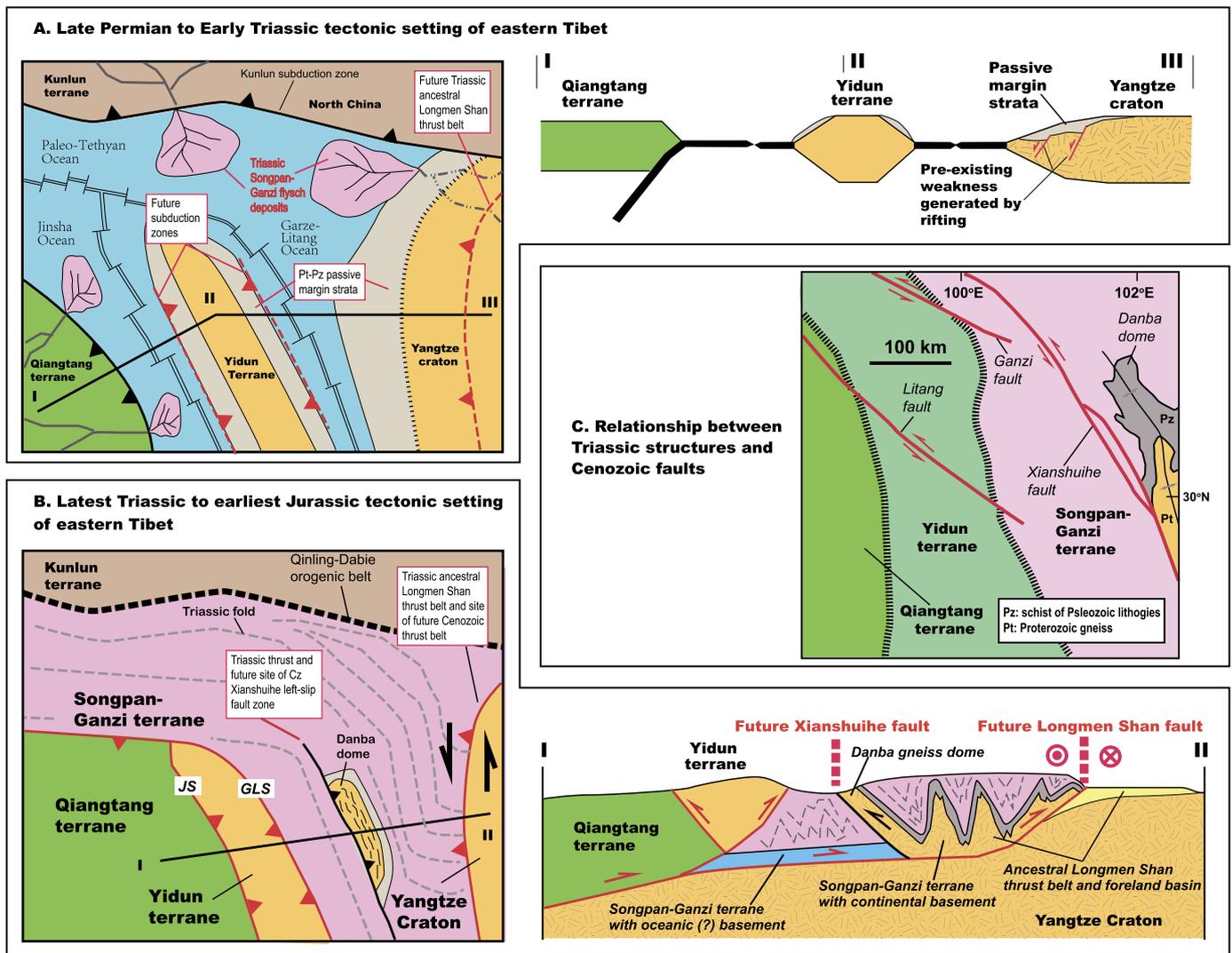
Fig. 2. Tectonic evolution of eastern Tibet from the late Permian to the latest Triassic. (A) Map and cross-section views of the tectonic setting of eastern Tibet in the Permian. During this time the Yidun terrane as a continental strip was rifted away from the Yangtze terrane of South China block. The rifting event was followed by the opening of the Garze–Litang ocean. The map is modified from Reid et al. (2005). (B) Map and cross section views of the tectonic setting in the Late Triassic in eastern Tibet. The Garze–Litang oceanic lithosphere started subducting below the Yidun terrane in the Latest Permian and Early Triassic, leading to the ocean closure at the end of the Triassic (Reid et al., 2005). The western margin of the Yangtze terrane experienced compressional tectonics, leading to the juxtaposition of deep-water continental-slope deposits over the cratonal sequence of the Yangtze terrane (Burchfiel et al., 1995). In this study, we infer that the Danba antiform and its related thrust mark the boundary between the Yangtze terrane with a continental basement and the Songpan–Ganzi terrane with an oceanic basement. This Triassic boundary was reactivated to form the Cenozoic Xianshuihe fault. (C) Relationship between the Cenozoic Xianshuihe fault and the Danba gneiss dome after Roger et al. (2010). (For interpretation of the colors in the figure(s), the reader is referred to the web version of this article.)

et al., 2014). The northwest-striking Xianshuhe fault is linked with the north–northwest-striking Anninghe fault, which in turn links with the north-striking Xiaojiang fault, from north to south (Fig. 1). This systematic change in fault orientation without a change in fault kinematics may have resulted from clockwise rotation of several crustal fragments in eastern Tibet due to the Cenozoic northward indentation of India into Asia (Burchfiel et al., 1995; Royden et al., 1997).

2.3. Relationships between Triassic and Cenozoic structures

The active left-slip Xianshuihe fault bounds the southwestern edge of the Danba gneiss dome (Fig. 2C), which has a complex history of deformation, metamorphism, and magmatism from the latest Permian to the earliest Jurassic (Huang et al., 2003; Zhou et al., 2008). The dome consists of a metamorphic core of Proterozoic gneiss juxtaposed on top by a warped ductile shear

zone against overlain by a sequence of Ordovician–Triassic low-grade sedimentary strata (Zhou et al., 2008).

In the Longmen Shan region, the Triassic deformation is expressed by broad left-slip shear deformation as indicated by the systematic deflection of fold-trace trends and thrusting characterized by juxtaposition of deep-water Neoproterozoic to Triassic deposits over the cratonal sequence of the Yangtze terrane (Burchfiel and Chen, 2012). It is at this Triassic deformation domain along the western margin of the Yangtze terrane where the active Longmen Shan thrust belt was initiated. Its reactivation along the Triassic structures is best expressed by its parallel and spatially overlapping relationship to the 1000-km long north-trending belt of Triassic gneiss domes (Zhou et al., 2008). The field relationship of Paleozoic–Mesozoic strata over the Cenozoic fold-and thrust belt in the central part of the eastern Longmen Shan is interpreted to indicate reactivation of the Triassic thrust decollement by Cenozoic deformation (Burchfiel et al., 1995).
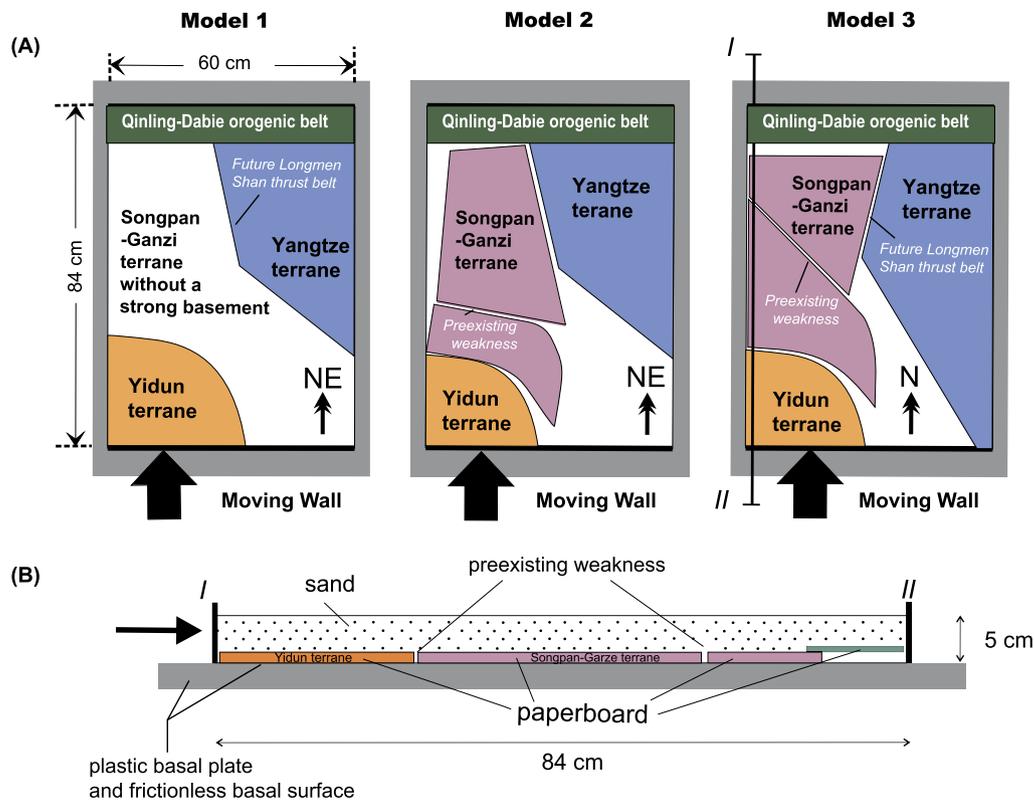
Fig. 3. Pre-Cenozoic basement configurations adopted in this study. (A) Three models are considered. (1) Model 1 assumes no strong basement below the Songpang–Ganzi terrane and the Cenozoic deformation is induced by northeast–southwest compression. (2) Model 2 assumes the northern part of the Songpan–Ganzi terrane has a strong basement whereas the southern part does not. Cenozoic deformation in the region is induced by northeast–southwest compression. In addition, the strong basement of the northern Songpan–Ganzi terrane has two fragments, with the boundary following the current trace of the Xianshuihe fault. (3) Model 3 assumes the northern part of the Songpan–Ganzi terrane has a strong basement whereas the southern part does not. Cenozoic deformation in the region is induced by north–south rather than northeast–southwest compression as assumed in models 1 and 2. The strong basement of the northern Songpan–Ganzi terrane consists of two fragments and their boundary follows the current trace of the Xianshuihe fault. (B) Cross section along the left margin of model 2 to show the locations of preexisting weakness.

Table 1
Scaling relationships used in the analogue experiments.

	Model	Nature	Model/Nature
Thickness	5 (cm)	∼30 (km)	1.67×10^{-6}
Length	84 (cm)	∼500 (km)	1.67×10^{-6}
Width	60 (cm)	∼360 (km)	1.67×10^{-6}
Density	1.56×10^3 (kg/m^3)	2.7×10^3 (kg/m^3)	5.78×10^{-1}
Convergence time	1600 (s)	30 (Ma)	1.71×10^{-12}
Shortening magnitude	160 (mm)	∼100 (km)	2.67×10^{-7}

3. Analogue models

3.1. Experimental materials and scaling relationships

A sandbox experimental apparatus hosted in the Tectonic Modeling Laboratory of China University of Geosciences (Beijing) was used to perform all the experiments. The sandbox has two fixed sidewalls and a fixed end wall, and convergence is initiated by a moving back wall (Fig. 3A). Dry quartz sand with grain size 125–225 μm was used in the experiments to represent the brittle crust in eastern Tibet. The sand has a coefficient of internal friction $\mu \approx 0.60$ (with an angle of internal friction $\varphi \approx 31°$) and a cohesive strength $C \approx 40–70$ Pa, which are similar to those estimated by Zuza et al. (2017). Our sand has a density of $\rho \approx 1560$ g/m^3 (Table 1). Deformation histories of the sandbox experiments are recorded as digital images using a Canon 500D camera. A commercially available two-dimensional particle image velocimetry (PIV) system (http://www.piv.com.cn/) was employed to convert the image history to a sand-particle velocity-field history. The algorithm of conversion is based on cross correlation of a pair of two singly exposed images using a multi-pass and multi-grid function method. The method follows the general schemes outlined in Adam et al. (2005) and Raffel et al. (2007) with additional elements from Pan et al. (2013) for more efficient computation. As the recorded displacements are much greater than the sand grain sizes, the uncertainty of the determined velocity values measured by standard deviation is rather small, typically in the range of ∼1% of the mean velocity values when compared against results derived from images generated by Monte Carlo simulations.

Relating the analogue experiments to crustal-scale deformation requires dynamic and geometric scaling that is governed by the following relationship (Hubbert, 1937):

$$\frac{C^{model}}{C^{nature}} = \frac{\sigma_V^{model}}{\sigma_V^{Nature}} = \frac{\rho^{model} \times L^{model} \times g^{model}}{\rho^{nature} \times L^{nature} \times g^{nature}} \quad (1)$$

where C is cohesive strength, σ_V is vertical normal stress, ρ is the density, L is the dimension, and g is gravitational acceleration; the superscript denotes the analogue-model vs. real-world (nature) parameters. If we take rock cohesive strength C^{model} to

be 70 MPa (Jaeger et al., 2009), we arrive at a geometric scaling factor between sand and crust as $\frac{L^{model}}{L^{nature}} \approx \sim 1.73 \times 10^{-6}$. Accordingly, 1 cm sand thickness in our experiment represents ∼6 km crustal thickness. Our experiments, which use a sand-layer thicknesses of 5 cm and horizontal dimensions of 84 cm × 60 cm, represents about an upper crustal section that is 30 km thick with a 500 km × 360 km horizontal dimension (Table 1). In all the experimental results presented below, we focus on the interactions between the Xianshuihe fault system and Longmen Shan fault system. In this context, the development of the eastern Tibetan plateau was created by a total of ∼100 km shortening either in the north–south or northeast–southwest direction over the past 30 Ma, which corresponds to a shortening of rate of ∼3.3 mm/yr (Table 1). The total shortening magnitude is consistent with the estimated Cenozoic shortening (Hubbard and Shaw, 2009) and the averaged Late Cenozoic slip rates across the Longmen Shan region (Burchfiel et al., 1995).

3.2. Model setup

In order to evaluate the effects of preexisting weakness on the Cenozoic evolution of eastern Tibet, we treat basement geometry and shortening direction as variables. To this end we use pre-cut paperboard to represent the strong basal section of the upper crust, which is overlain by sand to represent the crustal rocks and underlain by nearly frictionless plastic sheet to represent viscous lower crust whose strength does not interfere with the structural development of the upper crust. The basement shape of the Yidun terrane (orange), the Sichuan basin of the Yangtze terrane (blue), and the Qinling–Dabie orogen (dark green) is shown in Fig. 3A for three models examined in this study. In the first case, the sand rests directly on top of the basal plastic sheet in the region representing the Songpan–Ganzi terrane, which implies that the Songpan–Ganzi terrane lacks a strong basement and its crust has a uniform mechanical strength (see model 1 in Fig. 3A). In model 2, we use two pieces of paperboard to represent the strong basement of the Songpan–Ganzi terrane; the boundary between the two "basement fragments" represents the Triassic thrust bounding the Danba dome as shown in Fig. 2 (see model 2 in Fig. 3A). For both models 1 and 2, the compressional direction is northeast–southwest. In model 3, we use the trend of the Longmen Shan thrust belt as a reference and change the shortening direction to north–south while maintaining the same basement configuration (see model 3 in Fig. 3A). The relationship among the basement fragments in model 3 is shown in Fig. 3B.

4. Experimental results

The experimental results are displayed as images of deformation patterns, vorticity distribution, and spatial variation of northeastward velocity magnitude as shown in Figs. 4 and 5. The results allow us to compare the model results against the known geologic relationships in eastern Tibet, which we discuss below. The final fault pattern generated by model 1 was produced by northeastward push with the Songpan–Ganzi terrane lacking a strong basement across eastern Tibet as shown in panel (1) of Fig. 3A. The deformation map shows the formation of an arc-shaped thrust belt across the western margin of the Songpan–Ganzi terrane but lacking northwest-striking left-slip faults, which is not consistent with the Cenozoic tectonics of eastern Tibet (Figs. 1 and 2C). Along the boundary between the Songpan–Ganzi and Yangtze terranes, the model 1 experiment does produce a northeast-striking thrust zone that has a minor right-slip offset. Even though this is consistent with the location and the kinematics of the Cenozoic Longmen Shan thrust belt, the extent of the fault zone generated by the

model is too restricted to the south to match the observations (Fig. 4A, cf. Fig. 1).

The final deformation pattern generated by model 3 (Fig. 4C) also does not match the observations from eastern Tibet. The model assumes a two-piece strong basement in the north and weak basement in the south for the Songpan–Ganzi terrane in eastern Tibet under persistence north–south shortening. Experiment from this model creates a northwest-striking right-slip shear zone along the boundary of the two basement fragments beneath the northern part of Songpan–Ganzi terrane and a northeast-striking left-slip shear zone along the boundary between the Songpan–Ganzi and Yangtze terrane. Although the model is able to produce fault zones at the locations of the Xianshuihe fault zone and the Longmen Shan thrust belt in eastern Tibet, its predicted fault kinematics is inconsistent with the observed fault kinematics (Fig. 4C; cf. Fig. 1).

Among the experimental results from the three models, only model 2 assuming a two-piece strong basement in the north and a weak basement in the south for the Songpan–Ganzi terrane in eastern Tibet produces deformation that is compatible with the observations (Fig. 4B). In this model, persistent northeast–southwest shortening is applied, which creates a northwest-striking left-slip shear zone along the weakness within the two-piece basement and a northeast-striking right-slip transpressional shear zone along the boundary between the Songpan–Ganzi and Yangtze terranes (Fig. 4B; cf. Fig. 1).

Because of the success of model 2 in predicting the current fault pattern in eastern Tibet, we describe in detail below how the structural pattern has evolved with time measured by fraction of the total northward push (= 16 cm) (Fig. 5). To illustrate this, we divide the deformation history of the model 2 experiment into five stages.

Stage 1. Panel 1 of Fig. 5A displays the deformation pattern whereas panel 1 of Fig. 5B shows the vorticity distribution (positive for left-slip shear and negative for right-slip shear) across the portion of the total modeled area representing the region covering the Xianshuihe and Longmen Shan fault zones. The corresponding boundary condition is 2% of the total 16-cm northeastward push. At this stage, a subtle but recognizable northeast-striking right-slip shear zone is developed along the boundary between the Songpan–Ganzi and Yangtze terranes, as indicated by the deflection of the originally straight strain marker lines (panel 1 in Fig. 5A). Although there are no observable surface breaks along this shear zone, the localization of right-slip shear deformation is clearly shown in the vorticity map and the northeastward velocity modeled map in panel 1 of Fig. 5B and panel 1 of Fig. 5C, respectively. A northwest-striking shear zone can also be recognized in the velocity map in panel 1 of Fig. 5C, which cannot be detected from the image of surface deformation (panel 1 of Fig. 5A) and the corresponding vorticity map (panel 1 of Fig. 5B). The upper-left corner of the image displays a northeast-striking left-slip transpressional shear zone. The feature is an artificial edge effect of shear deformation between soft sand and rigid paperboard along the left side wall of our model setup (see Fig. 5D). This artefact is also shown in the vorticity map in panel 1 of Fig. 5B as a narrow left-slip shear zone.

Stage 2. The deformation pattern corresponding to 30% of the total 16-cm northward push is illustrated in panel 2 of Fig. 5A. A right-slip transpressional duplex system (Woodcock and Fischer, 1986) along the southern segment and a transpressional system consisting of two parallel faults along the northern segment of the northeast-striking right-slip shear zone imaged in panel 1 of Fig. 5 are now fully developed. Note that one of the two parallel faults (F2) in the north along the fault zone is dominantly right-slip, whereas the other fault (F3) is dominantly reverse-slip (panel 2 of Fig. 5A). The vorticity map shows intensified right-slip shear
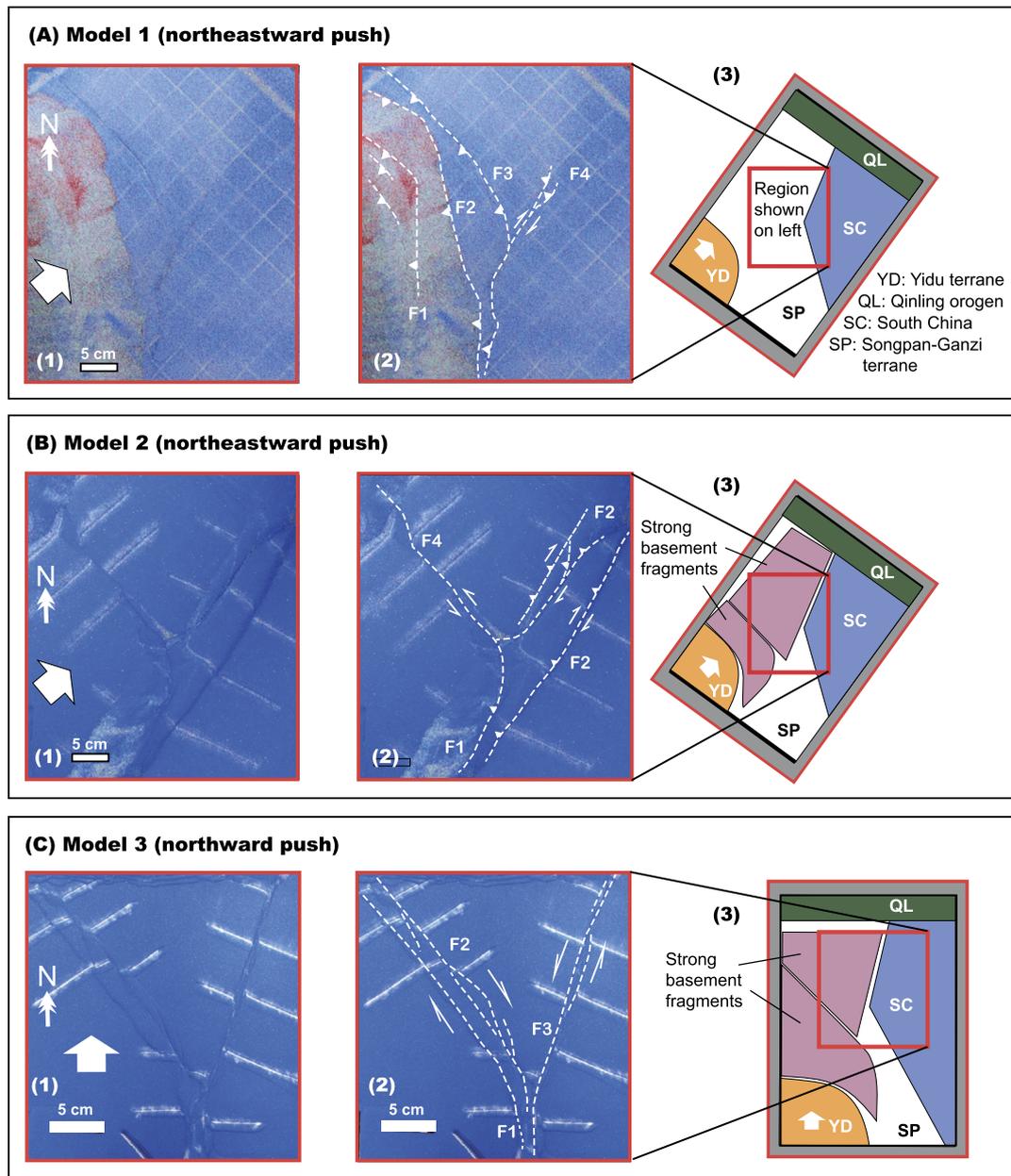
Fig. 4. Comparison of the final deformation pattern among models 1 (A), 2 (B), and 3 (C). The three panels in (A), (B) and (C) represent (1) an image without interpreted fault lines, (2) the same image with interpreted fault lines, and (3) the location of the image in the model area. Note that the results of models 1 and 2 were produced by northeastward push, whereas result of model 3 was generated by northward push.

in the north but weakened right-slip shear in the south along the through-going northeast-striking shear zone cutting the model area into two halves (panel 2 of Fig. 5B). The transition of the two fault segments along the northeast-striking shear zone is marked by the intersection of this fault zone with a northwest-striking shear zone along the preexisting weakness of the two-piece basement of the Songpan–Ganzi terrane. This shear zone is only detectable in the velocity distribution map (panel 2 of Fig. 5C) and subtly expressed as a northwest-trending shear zone in the vorticity map (panel 2 of Fig. 5B). Again, the upper left corner of the image displays a left-slip transpressional shear zone (see panel 2 of Fig. 5A and panel 2 of Fig. 5B), which is the artificial edge effect of our model setup.

Stage 3. While right-slip shear deformation continues along F1 and F2 segments of the northeast-striking fault zone at the modeled western edge of the Yangtze terrane, the northern part of F3 is now dominated by right-slip motion whereas the southern part

of F3 remains thrust-dominated (panel 3 of Figs. 5A, 5B, and 5C). Also note that the northwest-striking left-slip fault along the weak contact of the two basement fragments in the northern Songpan–Ganzi terrane is fully developed and recognizable by surface offsets of strain markers (panel 3 of Fig. 5A). The vorticity and velocity distribution maps show further intensification in the north and weakening in the south of the right-slip shear along the northeast-striking fault zone consisting of F1, F2, and F3 (panels 3 of Figs. 5B and 5C).

Stage 4. While all the faults maintain their earlier kinematics as shown in stage 3, F1 has changed its original right-slip transpressional kinematics to become a thrust system linking with the southern segment of thrust fault F4 (panel 4 of Fig. 5A). This conversion again is indicated by the weakening of the right-slip shear south of the intersection of the northwest-striking and northeast-striking fault zones (panels 4 of Figs. 5B and 5C). Meanwhile, the northwest-striking left-slip shear zone is fully developed as a
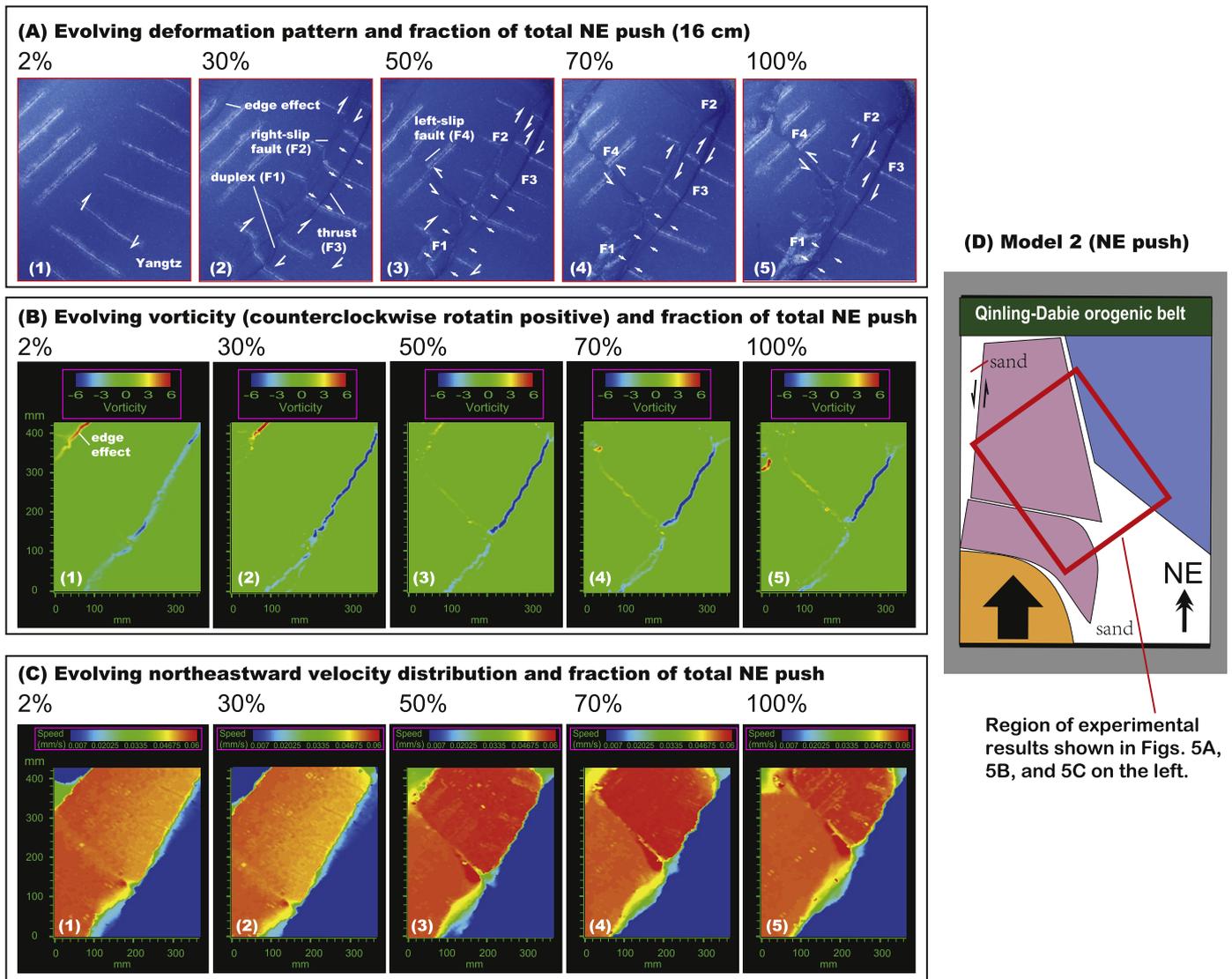
Fig. 5. Results of model 2 experiments assuming a two-piece strong continental basement below the northern part of the Songpan–Ganzi terrane in eastern Tibet. (A) Deformation history as a result of increasing shortening measured by the fraction of total northeastward push (16 cm). (B) Evolution of vorticity distribution across the modeled area and its relationship to fraction of total northward push. Note that the left-slip shear in the upper-left corner is an artificial edge effect of the model as discussed above. (C) Northeastward velocity magnitude as a function of the fraction of the total northward push. The sharp boundaries between high and low velocity magnitudes mark the locations of major shear zones.

through-going feature with minor sub-parallel branches (panel 4 of Fig. 5A).

Stage 5. When compared against fault patterns and vorticity maps shown in stages 2, 3, and 4, it is noticeable that the active portion of the northern right-slip segment of fault 3 (F3) has progressively shortened, with its northernmost part becoming deactivated with time. This is best shown in panel 5 of Fig. 5B where the intensity of shear strain (vorticity) becomes undetectable along the northern end of the fault trace. Meanwhile, the vorticity intensifies along the northwest-striking left-slip fault zone. As a result of left-slip movement, Fault 1 (F1), the original right-slip transpressional duplex at the southern end of the northeast-striking fault zone is now fully converted into a thrust zone accommodating northwest–southeast shortening (panel 5 of Fig. 5).

5. Discussion and conclusions

The results of our analogue modeling show that the geometry and spatial distribution of basement rocks below major tectonic terranes in eastern Tibet may have played a decisive role in con-

trolling the orientations of the complex fault zones in the area. In addition, the kinematics of the Cenozoic fault zones reactivated from pre-existing weakness in the crust is critically dependent on the boundary conditions (i.e., the direction of the principal shortening strain axis) along the southern edge of eastern Tibet. As describe above, our best model is the one that assumes a two-piece strong basement in the north and a weak basement in the south for the Songpan–Ganzi terrane in eastern Tibet under northeast–southwest compression. Without these two conditions, one dealing with the pre-existing basement flaws and another with a specific boundary condition, we were unable to produce the observed Cenozoic fault pattern and kinematics in eastern Tibet.

Our inferred northeast–southwest compression persistent in the past 30 Ma across eastern Tibet is consistent with the results of early studies such as that of Ratschbacher et al. (1996). These researchers shown that the northeastern corner of the Indian continent against the eastern Himalayan syntaxis and the southwestern corner of the Sichuan basin have been approaching one another in the Late Cenozoic, causing northeast–southwest shortening as a result of the Cenozoic India–Asia collision. A similar conclusion was
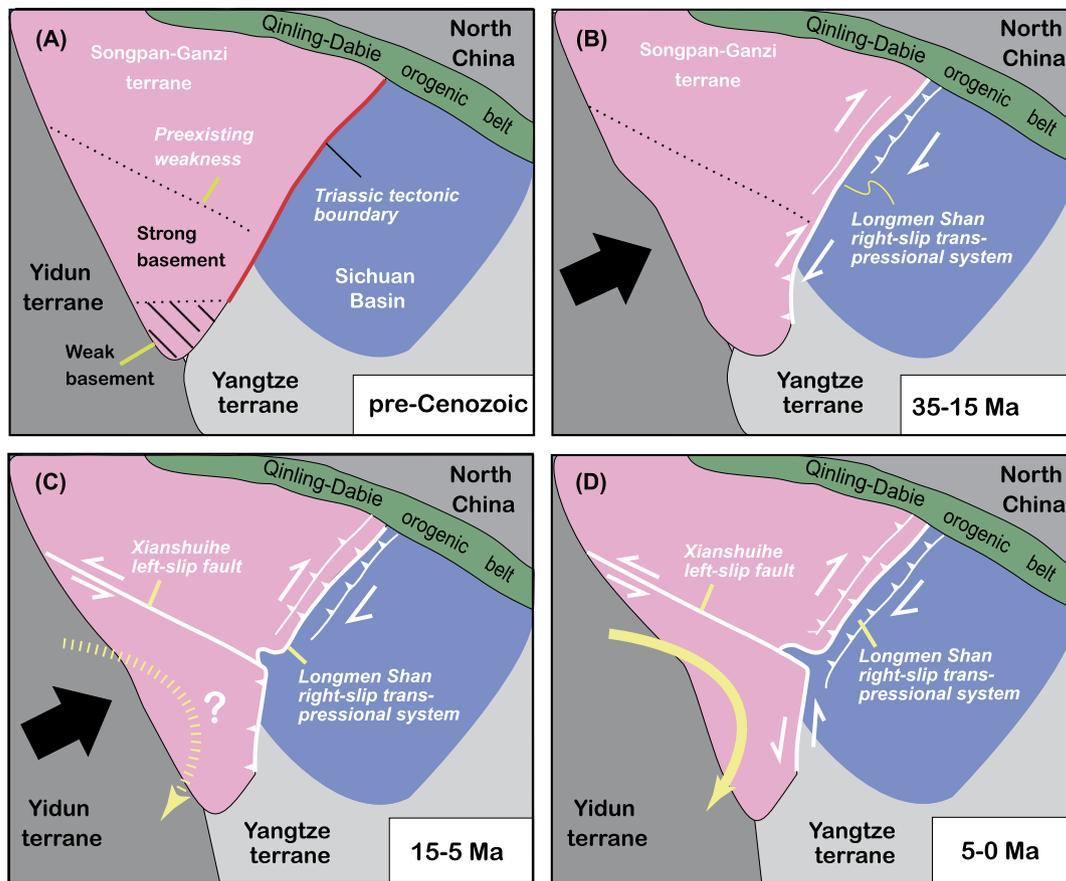
Fig. 6. Tectonic evolution of eastern Tibet based on the results of our analogue model experiments and the existing geological constraints. See text for details.

also reached by Hallet and Molnar (2001) inferred from the abnormal drainage pattern across southeast Tibet. Finally, our inferred northeast–southwest compression for reactivating pre-existing Triassic tectonic structures is consistent with the strain-rate tensors determined from GPS surveys across eastern and southeast Tibet (Gan et al., 2007).

Despite the successful prediction of the orientations and kinematics of the Xianshuihe and Longmen Shan fault zones in eastern Tibet, our preferred model (model 2) failed to produce left-slip faulting along the north-trending southern margin of the Yangtze terrane, where the active left-slip Anninghe and Xiaojiang faults are located. We believe that this problem is due to our model setup, which did not rotate the Yidun terrane while it moves northeastward, a history implied by the regional geologic synthesis of Burchfiel et al. (1995) and Burchfiel and Chen (2012). However, our model does correctly predicts the sequence of deformation between the Longmen Shan fault zone and the Xianshuihe fault zone, with the latter as the youngest structure dominated by left-slip transpressional deformation as suggested by Burchfiel et al. (1995). Our model also shows that motion of the Xianshuihe fault modifies the geometry and kinematics of the southernmost Longmen Shan thrust belt, another prediction that is consistent with the geologic observation documented in Burchfiel et al. (1995).

Based on the regional geologic synthesis of Burchfiel et al. (1995) and Burchfiel and Chen (2012) and the results of our analogue experiments, we propose the following kinematic model for the evolution of the eastern Tibetan plateau. Immediately prior to Cenozoic deformation, the region is dominated by the following tectonic terranes that are bounded by major tectonic boundaries as pre-existing weakness: the Yidun terrane, the Songpan–Ganzi terrane with a strong two-piece basement in the north and a weak basement in the south, and the Yangtze terrane (Fig. 6A).

From ∼35 Ma to 15 Ma, the initial Longmen Shan right-slip transpressional system was developed (Wang et al., 2014), which follows the Triassic ancestral Longmen Shan transpressional zone of Burchfiel et al. (1995) (Fig. 6B). As a result of continuous northeast–southwest shortening between 15 and 5 Ma, possibly coupled with clockwise rotation across eastern and southeast Tibet, the weakness of the Songpan–Ganzi basement became reactivated, forming the northwest-striking left-slip Xianshuihe fault zone that links with the southern segment of the original Longmen Shan right-slip transpressional belt (Fig. 6C). As a result of initial left-slip faulting along the Xianshuihe fault it is possible that the Anninghe and Xianjiang faults were originally thrusts of the southern Longmen Shan fault zone as predicted by our model. The assumption of northeast–southwest compression in our model is an oversimplification, as the coupled clockwise rotation of major crustal blocks could have been an additional driver for the initiation of the curved Xianshuihe–Anninghe–Xiaojiang fault zone as shown in Fig. 6C. The final stage of deformation from 5 Ma to the present may have been dominated by clockwise of southeast Tibet as indicated by the GPS studies (Gan et al., 2007) (Fig. 6D). Our kinematic model emphasizes the role of pre-existing structural anisotropy in controlling the tectonic development of the Tibetan plateau, a conclusion that was also reached by numerical modeling considering the pre-existing weakness as possible reactivation sites of Cenozoic structures (Kong et al., 1997).

tailed review by Saad Haq that greatly improved the rigor and presentation of this paper.

References

Adam, J., Urai, J.L., Wieneke, B., Oncken, O., Pfeiffer, K., Kukowski, N., Lohrmann, J., Hoth, S., Van Der Zee, W., Schmatz, J., 2005. Shear localisation and strain distribution during tectonic faulting—new insights from granular-flow experiments and high-resolution optical image correlation techniques. J. Struct. Geol. 27 (2), 283–301.

Bendick, R., Flesch, L., 2007. Reconciling lithospheric deformation and lower crustal flow beneath central Tibet. Geology 35 (10), 895–898.

Burchfiel, B.C., Chen, Z.L., 2012. Tectonics of the Southeastern Tibetan Plateau and its adjacent foreland. Mem. Geol. Soc. Amer. 210, 1–164.

Burchfiel, B.C., Zhiliang, C., Yupinc, L., Royden, L.H., 1995. Tectonics of the Longmen Shan and adjacent regions, central China. Int. Geol. Rev. 37 (8), 661–735.

Clark, M.K., Royden, L.H., 2000. Topographic ooze: building the eastern margin of Tibet by lower crustal flow. Geology 28 (8), 703–706.

Cooke, M.L., Underwood, C.A., 2001. Fracture termination and step-over at bedding interfaces due to frictional slip and interface opening. J. Struct. Geol. 23 (2), 223–238.

de Sigoyer, J., Vanderhaeghe, O., Duchêne, S., Billerot, A., 2014. Generation and emplacement of Triassic granitoids within the Songpan Ganze accretionary-orogenic wedge in a context of slab retreat accommodated by tear faulting, Eastern Tibetan plateau, China. J. Asian Earth Sci. 88, 192–216.

England, P., Houseman, G., 1989. Extension during continental convergence, with application to the Tibetan Plateau. J. Geophys. Res., Solid Earth 94 (B12), 17561–17579.

Gan, W., Zhang, P., Shen, Z.K., Niu, Z., Wang, M., Wan, Y., Cheng, J., 2007. Present-day crustal motion within the Tibetan Plateau inferred from GPS measurements. J. Geophys. Res., Solid Earth 112 (B8).

Hallet, B., Molnar, P., 2001. Distorted drainage basins as markers of crustal strain east of the Himalaya. J. Geophys. Res., Solid Earth 106 (B7), 13697–13709.

Haq, S.S., Davis, D.M., 1997. Oblique convergence and the lobate mountain belts of western Pakistan. Geology 25 (1), 23–26.

Hawkesworth, C.J., Cawood, P.A., Dhuime, B., Kemp, T.I., 2017. Earth's continental lithosphere through time. Annu. Rev. Earth Planet. Sci. 45 (1), 169–198.

Huang, M., Maas, R., Buick, I.S., Williams, I.S., 2003. Crustal response to continental collisions between the Tibet, Indian, South China and North China blocks: geochronological constraints from the Songpan–Garze orogenic belt, western China. J. Metamorph. Geol. 21 (3), 223–240.

Hubbard, J., Shaw, J.H., 2009. Uplift of the Longmen Shan and Tibetan plateau, and the 2008 Wenchuan (M = 7.9) earthquake. Nature 458, 194–197.

Hubbert, M.K., 1937. Theory of scale models as applied to the study of geologic structures. Geol. Soc. Am. Bull. 48 (10), 1459–1520.

Jaeger, J.C., Cook, N.G., Zimmerman, R., 2009. Fundamentals of Rock Mechanics. John Wiley & Sons.

Kluth, C.F., Coney, P.J., 1981. Plate tectonics of the ancestral Rocky Mountains. Geology 9 (1), 10–15.

Kong, X., Yin, A., Harrison, T.M., 1997. Evaluating the role of preexisting weaknesses and topographic distributions in the Indo-Asian collision by use of a thin-shell numerical model. Geology 25 (6), 527–530.

Liu-Zeng, J., Wen, L., Sun, J., Zhang, Z., Hu, G., Xing, X., Xu, Q., 2010. Surficial slip and rupture geometry on the Beichuan fault near Hongkou during the Mw 7.9 Wenchuan earthquake, China. Bull. Seismol. Soc. Am. 100 (5B), 2615–2650.

McKenzie, D., Jackson, J., Priestley, K., 2005. Thermal structure of oceanic and continental lithosphere. Earth Planet. Sci. Lett. 233 (3), 337–349.

Neil, E.A., Houseman, G.A., 1997. Geodynamics of the Tarim Basin and the Tian Shan in central Asia. Tectonics 16 (4), 571–584.

Nie, S., Yin, A., Rowley, D.B., Jin, Y., 1994. Exhumation of the Dabie Shan ultra-high-pressure rocks and accumulation of the Songpan–Ganzi flysch sequence, central China. Geology 22 (11), 999–1002.

Pan, B., Li, K., Tong, W., 2013. Fast, robust and accurate digital image correlation calculation without redundant computations. Exp. Mech. 53 (7), 1277–1289.

Raffel, M., Willert, C.E., Kompenhans, J., 2007. Particle Image Velocimetry: A Practical Guide. Springer Science & Business Media, p. 445.

Ratschbacher, L., Frisch, W., Chen, C., Pan, G., 1996. Cenozoic deformation, rotation, and stress patterns in eastern Tibet and western Sichuan, China. In: Yin, A., Harrison, T.M. (Eds.), The Tectonic Evolution of Asia. Cambridge Univ. Press, New York, pp. 227–249.

Reid, A.J., Wilson, C.J., Liu, S., 2005. Structural evidence for the Permo-Triassic tectonic evolution of the Yidun Arc, eastern Tibetan Plateau. J. Struct. Geol. 27 (1), 119–137.

Roger, F., Calassou, S., Lancelot, J., Malavieille, J., Mattauer, M., Xu, Z.Q., Hao, Z.W., Hou, L.W., 1995. Miocene emplacement and deformation of the Konga Shan granite (Xianshui He fault zone, west Sichuan, China): geodynamic implications. Earth Planet. Sci. Lett. 130, 201–216.

Roger, F., Jolivet, M., Malavieille, J., 2010. The tectonic evolution of the Songpan–Garzê (North Tibet) and adjacent areas from Proterozoic to Present: a synthesis. J. Asian Earth Sci. 39 (4), 254–269.

Royden, L.H., Burchfiel, B.C., King, R.W., Wang, E., Chen, Z., Shen, F., Liu, Y., 1997. Surface deformation and lower crustal flow in eastern Tibet. Science 276 (5313), 788–790.

Taylor, M., Yin, A., 2009. Active structures of the Himalayan–Tibetan orogen and their relationships to earthquake distribution, contemporary strain field, and Cenozoic volcanism. Geosphere 5 (3), 199–214.

Tong, H., Yin, A., 2011. Reactivation tendency analysis: a theory for predicting the temporal evolution of preexisting weakness under uniform stress state. Tectonophysics 503 (3), 195–200.

Viola, G., Odonne, F., Mancktelow, N.S., 2004. Analogue modelling of reverse fault reactivation in strike-slip and transpressive regimes: application to the Giudicarie fault system, Italian Eastern Alps. J. Struct. Geol. 26 (3), 401–418.

Wang, E., Meng, K., Su, Z., Meng, Q., Chu, J.J., Chen, Z., Wang, G., Shi, X., Liang, X., 2014. Block rotation: tectonic response of the Sichuan basin to the southeastward growth of the Tibetan Plateau along the Xianshuihe–Xiaojiang fault. Tectonics 33 (5), 686–718.

Woodcock, N.H., Fischer, M., 1986. Strike-slip duplexes. J. Struct. Geol. 8 (7), 725–735.

Yan, D.P., Zhou, M.F., Li, S.B., Wei, G.Q., 2011. Structural and geochronological constraints on the Mesozoic–Cenozoic tectonic evolution of the Longmen Shan thrust belt, eastern Tibetan Plateau. Tectonics 30, TC6005–TC6028.

Yan, D.P., Xu, Y.B., Dong, Z.B., Qiu, L., Zhang, S., Wells, M., 2016. Fault-related fold styles and progressions in fold-thrust belts: insights from sandbox modeling. J. Geophys. Res., Solid Earth 121, 2087–2111. https://doi.org/10.1002/2015JB012397.

Yin, A., Harrison, T.M., 2000. Geologic evolution of the Himalayan–Tibetan orogen. Annu. Rev. Earth Planet. Sci. 28 (1), 211–280.

Yin, A., Nie, S., 1996. A Phanerozoic palinspastic reconstruction of China and its neighboring regions. In: Yin, A., Harrison, T.M. (Eds.), The Tectonics of Asia. Cambridge Univ. Press, New York, pp. 442–485.

Zhou, M.F., Yan, D.P., Kennedy, A.K., Li, Y., Ding, J., 2002. SHRIMP U–Pb zircon geochronological and geochemical evidence for Neoproterozoic arc-magmatism along the western margin of the Yangtze block, South China. Earth Planet. Sci. Lett. 196, 51–67. https://doi.org/10.1016/S0012-821X(01)00595-7.

Zhou, M.F., Yan, D.P., Vasconcelos, P.M., Li, J.W., Hu, R.Z., 2008. Structural and geochronological constraints on the tectono-thermal evolution of the Danba domal terrane, eastern margin of the Tibetan plateau. J. Asian Earth Sci. 33 (5), 414–427.

Zuza, A.V., Yin, A., Lin, J., Sun, M., 2017. Spacing and strength of active continental strike-slip faults. Earth Planet. Sci. Lett. 457, 49–62.